# Adsorption of Ni(II) by a thermo-sensitive colloid: methylcellulose/calcium alginate beads

Zhongmin Li, Wanwan Wu, Wenyan Jiang, Guangtao Wei, Yunshang Li and Linye Zhang

## ABSTRACT

The adsorption of Ni(II) by a thermo-sensitive adsorbent of methylcellulose/calcium alginate beads (CAMCBs) was studied using batch adsorption tests to determine the adsorption process and properties, the effects of adsorbent dosage, initial concentration, adsorption time and temperature. The adsorption process was further investigated using kinetics, isotherms and thermodynamic methods. The kinetics and isotherms studies showed the adsorption of Ni(II) on CAMCBs was fitted by the pseudo-second-order kinetic model and Langmuir isothermal adsorption model, respectively. The thermodynamic parameters indicated that the adsorption process was spontaneous and exothermic at lower temperature, and the entropy of the adsorption process was negative. In the study of regeneration, it was confirmed that under the temperature of 60 °C, the desorption agent of $CaCl_2$ with concentration of 3 g·L$^{-1}$ was more conducive to the desorption of Ni(II) from CAMCBs. Both adsorption capacity and mechanical strength of the used CAMCBs could be basically recovered to the level of fresh CAMCBs after desorption. The prepared CAMCBs had a good property of adsorption of Ni(II) and an excellent regeneration performance.

**Key words** | adsorption, methylcellulose, Ni(II), sodium alginate, thermo-sensitive colloid

**Zhongmin Li**
**Wanwan Wu**
**Linye Zhang** (corresponding author)
Department of Energy Chemical Engineering,
Guangxi University,
Nanning,
China
E-mail: *yezi@gxu.edu.cn*

**Wenyan Jiang**
**Guangtao Wei**
**Yunshang Li**
Department of Chemical Engineering,
Guangxi University,
Nanning,
China

**Wenyan Jiang**
Agro-Products Quality, Safety and Testing Technology Research Institute,
Guangxi Academy of Agricultural Sciences,
Nanning,
China

## INTRODUCTION

Heavy metals are defined as metal elements with a relative atomic mass between 63.5 and 200.6 and a density greater than 5.0 kg·dm$^{-3}$. Nickel is one of the most common heavy metals in industrial effluents and is associated with toxicity problems. Heavy metals are well known to be harmful to most organisms when they are present in excessive concentrations. Hence, effective removal of toxic heavy metal ions from aqueous systems is of great importance for the protection of natural ecosystems. Many technologies have been used for removing Ni(II) from water, including chemical precipitation, membrane filtration, ion exchange, activated carbon adsorption and electrolysis. However, these conventional technologies have disadvantages, such as secondary pollution, short service life, low treatment capacity and high cost, and they are highly energy consuming (Zhou *et al.* 2017). Therefore, techniques that are low-cost, economic, effective, pollution-free and with high adsorption capacity are being widely studied and applied in the removal of Ni(II) from wastewater. Especially, biosorption is a viable alternative, with low cost, high efficiency, and minimization of waste generated during wastewater treatment (Volesky 1987).

Adsorbent selection, which determines the adsorption effect on the adsorbate, is very important in the application process of adsorption technology. At present, various adsorbents have been reported to remove heavy metal ions from industrial or agricultural wastewater, for example, active carbon (Depci *et al.* 2012), resins (Zhao *et al.* 2018), clays (Kara *et al.* 2017) and algae (Moino *et al.* 2017). In particular, algae biosorbents have attracted increased attention because

doi: 10.2166/aqua.2019.141

they involve lower investments in terms of both initial and running cost, simple design, easy operation and no effect of toxic substances on wastewater treatment.

Algae are divided into several absolutely independent evolutionary pathways: a 'red pathway' with red algae (*Rhodophyta*), a 'brown pathway' with brown algae (inter alia, *Chromophyta*) and a 'green pathway' that includes green algae (*Chlorophyta*) along with mosses, ferns and several plants (Romera *et al.* 2007). The brown variety has been studied most as a biosorbent because their cell walls contain biopolymer alginate, which is responsible for the mechanical strength and high adsorption capacity when compared with other algae. Sodium alginate (SA) is a renewable, anionic, linear natural polysaccharide and a major component of the cell walls of brown algae, and consists of the 1,4-linked C5 epimers, $\beta$-d-mannuronic acid (M or ManA) and $\alpha$-l-guluronic acid (G or GulA) found in homo or mixed blocks (Stender *et al.* 2018). Furthermore, SA has high reactive activities and can be easily modified by ionotropic gelation. For example, a low-cost and convenient way of crosslinking is immersing SA membranes into $CaCl_2$ solution for several minutes, thus the coupled $Ca^{2+}$ with oxygen molecule of the G sequences in the polymer chain build the 'egg-box structure', and the formation of insoluble calcium alginate follows (Xu *et al.* 2018). Insoluble alginate beads are widely used as biosorbents to adsorb various heavy metals through their carboxylic groups, and are convenient for separating the beads from wastewater after adsorption. Calcium alginate beads, one kind of alginate gels, have been reported in the literature to remove heavy metals. For instance, Hong *et al.* (2016) reported that calcium alginate beads showed an excellent adsorption performance for $Sr^{+}$; Ren *et al.* (2016) reported that the calcium alginate beads modified by adding carboxymethyl cellulose could increase the adsorption capacity for $Pb^{2+}$.

In addition, calcium alginate beads can be better removed from the treatment system after adsorption than SA when used as an adsorbent to adsorb dyes or heavy metal ions. However, there is not much research on the regeneration of calcium alginate except a few reports of using chemical reagents such as acids and salts (Hong *et al.* 2016). Therefore, SA is modified by polymer blending in this study; that is to say, the functional material methylcellulose (MC) is added to the sodium alginate aqueous solution, and the obtained mixture is added to $CaCl_2$ solution for calcification. MC is a natural carbohydrate polymer and freely soluble in water. It forms aqueous solutions and demonstrates a unique property to form reversible physical gels due to hydrophobic interactions when heated above a particular temperature (Ren *et al.* 2016). In theory, adding MC to SA can increase the adsorption capacity of colloid for Ni(II) from water and boost the difference of adsorption capacity between low and high temperatures. In other words, MC may be used in adsorbing, desorbing, and recovering Ni(II) by controlling the temperature. A thermo-sensitive colloid composed of calcium alginate and methylcellulose has been prepared in our lab, and it has been found that the methylcellulose/calcium alginate beads (CAMCBs) had a high capacity for adsorption of cationic dyes from wastewater (Li *et al.* 2016). Based on the results of adsorption of cationic dyes by CAMCBs and the characteristics of SA and MC, the prepared CAMCBs might also have a good adsorption ability for Ni(II) in water.

The aim of this paper was to provide the fundamental knowledge for adsorption of Ni(II) by the thermo-sensitive CAMCBs. The effects of various operating parameters have been investigated in detail. The process of Ni(II) adsorption by CAMCBs was investigated by kinetics, isotherms and thermodynamic methods. Furthermore, depending on the nature of the adsorbent and adsorbate, and also in order to maintain the structure of the adsorbent, $CaCl_2$ was chosen as the desorption agent to regenerate the used CAMCBs (Li *et al.* 2019), and the effect of $CaCl_2$ concentration on the desorption of Ni(II) was studied. In addition, the effects of regeneration times on the adsorption capacity and on the mechanical strength of CAMCBs were discussed as well.

## EXPERIMENT

### Materials

Sodium alginate and KI were purchased from Xilong Chemical Co. Ltd (Guangdong, China). Methylcellulose and anhydrous $CaCl_2$ were purchased from Sinopharm Chemical Reagent Co. Ltd (Shanghai, China). HCl, NaOH, $H_{12}N_2NiO_{12}$ and ammonium hydroxide were purchased

from Guanghua Science and Technology Co. Ltd (Guangdong, China). $C_4H_7N_3O_7$ and $I_2$ were purchased from Bodi Chemical Co. Ltd (Tianjin, China). $C_4H_8N_2O_2$ was purchased from East China normal university Chemical Plant (Shanghai, China). EDTA-$Na_2$ was purchased from Coolaber Science and Technology Co. Ltd (Beijing, China). All chemicals used in the study were of analytical reagent grade.

## Preparation of CAMCBs

First, 0.1 g of MC and 0.1 g of SA were added to 10 mL of deionized water at 30 °C, and then the mixed solution was placed in the ultrasound wave to remove the bubbles. After that, the formed MC/SA solution was added dropwise into 40 mL of $CaCl_2$ solution (5 wt%) under the stirring speed of 200 rpm; it took about 10 minutes for all MC/SA mixture to be dropped into $CaCl_2$ solution. Then the drops of MC/SA solution were calcified in the $CaCl_2$ solution. The calcified reaction was allowed to proceed for 4 h to form CAMCBs. Finally, the CAMCBs were separated from the solution and washed several times with deionized water, and then the CAMCBs were kept in deionized water to maintain their structure. The diameter of the prepared CAMCBs was about 2.0 mm.

## Characterization of adsorbent

The adsorbents before and after adsorption were characterized by scanning electron microscopy (SEM) and Fourier transform infrared spectroscopy (FT-IR). SEM micrographs of the adsorbents were recorded with a Hitachi S-3400N scanning electron microscope. FT-IR analysis was collected on a 1752X FT-IR spectroscopy using a KBr pellet in the range of 4,000–500 $cm^{-1}$ with 4 $cm^{-1}$ resolution.

Moreover, the mechanical strength of CAMCBs ($F$, N) was evaluated by the value of bearing force of CAMCBs which was recorded when the bead was pressed to a thickness of 0.8 mm in a hardness-testing device (Li *et al.* 2019).

## Adsorption/desorption of Ni(II) on CAMCBs and methods of measurement

A 100 mL quantity of Ni(II) solution with a certain concentration was added to a flask. The Ni(II) solution in the flask was kept at a desired temperature by controlling the temperature of the water bath. The prepared adsorbent was added to the flask at a magnetic stirring speed of 160 rpm. Solution samples were withdrawn from the flask at predetermined time intervals and were measured by a TU-1900 UV–vis spectrophotometer at 664 nm, which is the maximum absorbance wavelength of Ni(II). The solid-phase loading of Ni(II) ($q_t$, mg·$g^{-1}$) and the adsorption ratio of Ni(II) ($\eta$, %) were calculated as Equations (1) and (2), respectively.

$$q_t = \frac{(C_0 - C_t)V}{m} \tag{1}$$

$$\eta = \frac{(C_0 - C_t)}{C_0} \times 100\% \tag{2}$$

where $C_0$ (mg·$L^{-1}$) and $C_t$ (mg·$L^{-1}$) are the initial Ni(II) concentration and the Ni(II) concentration at time $t$ in adsorption experiment, respectively; $V$ (L) is the volume of Ni(II) solution, and $m$ (g) is the mass of adsorbent.

After the adsorption of Ni(II) the adsorbents were desorbed with 20 mL of different concentrations of $CaCl_2$ solution in the flask under the temperature of 60 °C. After desorption equilibrium, the final concentration of Ni(II) in the equilibrium solution was determined. The desorption mass of Ni(II) ($q_d$, mg·$g^{-1}$) and the desorption ratio of Ni(II) ($\eta_d$, %) were calculated as Equations (3) and (4), respectively.

$$q_d = VC_d \tag{3}$$

$$\eta_d = \frac{C_d}{(C_0 - C_e)} \tag{4}$$

where $C_d$ (mg·$L^{-1}$) is the equilibrium Ni(II) concentration in the desorption experiment and $C_e$ (mg·$L^{-1}$) is the equilibrium Ni(II) concentration in the adsorption experiment.

## Statistical analysis

All experiments were conducted in duplicates, and the mean results were obtained from these data. Linear regression was used to evaluate the fitness of the prediction models to the experimental data in this study using Origin 9.1. The suitability of the model fitting was assessed using $R^2$ values.

## RESULTS AND DISCUSSION

### Effects of adsorption conditions on adsorption of Ni(II) by CAMCBs

#### Effect of CAMCBs dosage on adsorption of Ni(II)

The adsorbent dosage is an important parameter in adsorption studies because it determines the capacity of adsorbent for a given initial concentration of Ni(II) solution. The effect of CAMCBs dosage on the adsorption of Ni(II) is shown in Figure 1(a). As seen from Figure 1(a), the adsorption capacity of Ni(II) decreased with the increase of CAMCBs dosage. A lower adsorbent dosage meant that a smaller overall total surface area of CAMCBs was exposed, and hence, more Ni(II) was adsorbed on the surface per gram unit of CAMCBs, which led to the higher adsorption capacity (Jalil *et al.* 2010). However, it was observed that the adsorption ratio initially increased rapidly and then almost reached a constant value after the CAMCBs dosage reached 2 g·L$^{-1}$. The adsorption ratio of Ni(II) increased from 55.1% to 69.6% with the dosage increase from 1 to 5 g·L$^{-1}$. The increase in adsorption ratio of Ni(II) was attributed to more available adsorption surface and more adsorption sites provided by added CAMCBs (Chen *et al.* 2010). Compared with that at the dosage of 2 g·L$^{-1}$, the adsorption ratio of Ni(II) showed no significant change when the dosage was over 2 g·L$^{-1}$. Therefore, following comprehensive consideration of changes in adsorption capacity and adsorption ratio with increasing dosage, 2 g·L$^{-1}$ of CAMCBs was chosen for later studies on the adsorption of Ni(II).

#### Effects of adsorption temperature and adsorption time on adsorption of Ni(II)

Temperature and time are both important parameters for the adsorption process, and the effects of temperature and time on the adsorption of Ni(II) on CAMCBs were investigated. As shown in Figure 1(b), the adsorption capacity of CAMCBs decreased with the increase of temperature in the range of 30 °C to 60 °C, which manifested that higher temperature was not conducive to the adsorption of Ni(II)

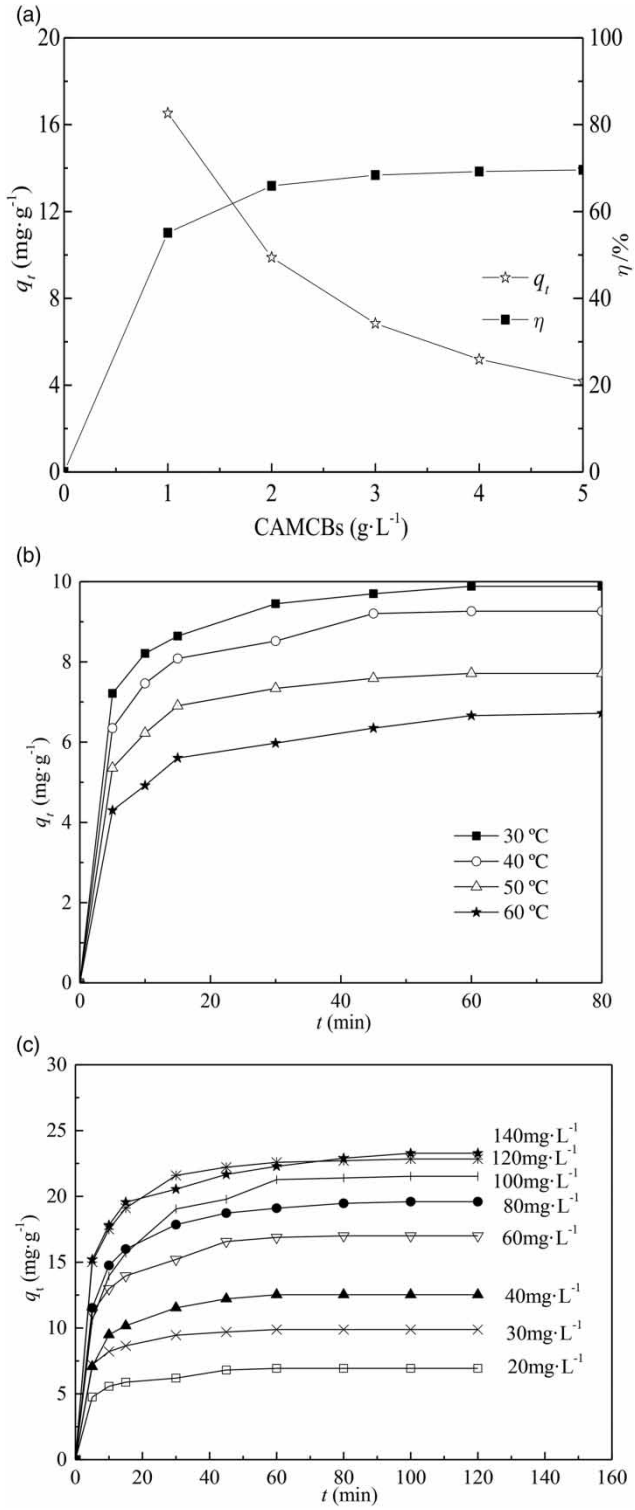


**Figure 1** | (a) Effect of CAMCBs dosage on adsorption of Ni(II) ($C_0$ = 30 mg·L$^{-1}$, T = 30 °C, t = 60 min, and initial pH = 6.9); (b) effects of adsorption temperature and adsorption time on adsorption of Ni(II) (dosage = 2 g·L$^{-1}$, $C_0$ = 30 mg·L$^{-1}$, and initial pH = 6.9); (c) effects of initial concentration and adsorption time on adsorption of Ni(II) (dosage = 2 g·L$^{-1}$, T = 30 °C, t = 60 min, and initial pH = 6.9).

on CAMCBs. The higher temperature significantly activated Ni(II) in the solution, which made it more difficult for Ni(II) to be adsorbed on the CAMCBs surface. Moreover, the higher temperature increased macromolecule cross-linking in the fiber, which narrowed the amorphous region and reduced the amount of Ni(II) that entered the fiber (Ren *et al.* 2016).

Furthermore, as shown in Figure 1(b) the adsorption capacity of Ni(II) on CAMCBs increased with the elapsed adsorption time and reached equilibrium as the adsorption time exceeded 60 min. This outcome suggested that the adsorption equilibrium time is approximately 60 min. It should be emphasized that the equilibrium time of this type of adsorbent was shorter than those reported in the literature (Xu *et al.* 2016; Liao *et al.* 2016).

### Effects of initial concentration and adsorption time on adsorption of Ni(II)

The effects of initial concentration of Ni(II) and adsorption time on the adsorption of Ni(II) were investigated. As shown in Figure 1(c), the maximum adsorption capacity of CAMCBs increased with the increase of initial Ni(II) concentration in the range of 20 to 140 mg·L$^{-1}$. When the initial Ni(II) concentration was higher, the adsorption rate increased quickly at first, and then went down slowly until the adsorption equilibrium. This was due to the fact that higher initial concentration of adsorbate provided more driving power of adsorption of Ni(II) on CAMCBs, which made the adsorbate easier to capture (Liao *et al.* 2016).

## Adsorption kinetics

In order to understand the adsorption mechanism and identify the potential rate controlling steps involved in the process of Ni(II) adsorption on CAMCBs, kinetic experimental data were analyzed and modeled by using three kinetic models: pseudo-first-order kinetic model (Equation (5)), pseudo-second order kinetic model (Equation (6)) and Bangham kinetic model (Equation (7)). The best-fit model was selected based on the linear regression correlation coefficient values ($R^2$).

$$\log(q_e - q_t) = \log q_e - \frac{k_1 t}{2.303} \tag{5}$$

$$\frac{t}{q_t} = \frac{1}{k_2 q_e^2} + \frac{t}{q_e} \tag{6}$$

$$\log\log\left(\frac{C_0}{C_0 - C_s q_t}\right) = \log\left(\frac{k_0 C_s}{2.303V}\right) + \alpha \log t \tag{7}$$

where $q_e$ (mg·g$^{-1}$) is the adsorption amount of Ni(II) on CAMCBs at equilibrium (values of calculated $q_e$ were obtained from Equation (7)), and $q_t$ (mg·g$^{-1}$) is the adsorption amount of Ni(II) on CAMCBs at time $t$. $k_1$ (min$^{-1}$) is the ratio constant of pseudo-first-order mode, and $k_2$ (g·mg$^{-1}$·min$^{-1}$) is the constant of pseudo-second-order mode. $C_S$ (g·L$^{-1}$) is the concentration of adsorbent. $\alpha$ and $k_0$ are the constant.

The pseudo-first-order equation, pseudo-second-order equation and Bangham equation were applied to fit the experimental data. Plots of pseudo-first-order, pseudo-second-order, and Bangham kinetic models under different temperatures and different Ni(II) initial concentrations are presented in Figures 2 and 3, respectively. Meanwhile, on the basis of the intercept and slope of the linear fitting, these kinetic model parameters could be calculated. These data are summarized in Tables 1 and 2, respectively. It can be found that the linear regression correlation coefficient values ($R^2$) with the pseudo-second-order model were higher ($R^2 > 0.995$ for all temperatures and initial concentrations) than the pseudo-first-order model, suggesting that the experimental data fitted better with the pseudo-second-order kinetic model than the pseudo-first-order model. A similar phenomenon has been observed in the adsorption of Ni(II) on chitosan (Liao *et al.* 2016) and novel silica-based hybrid adsorbents (Xu *et al.* 2016). In addition, comparison of $q_e$ values obtained via adsorption experiments with that obtained by linear fitting of the pseudo-second-order model showed that these values were similar. This result confirmed that the pseudo-second-order kinetic model can be used to describe the adsorption behavior of Ni(II) on CAMCBs. Moreover, plots of Figures 2(c) and 3(c) were found to be linear both for different temperatures and different Ni(II) initial concentrations, which confirmed that pore-diffusion was involved in Ni(II) adsorption onto CAMCBs (Namasivayam & Sangeetha 2006).

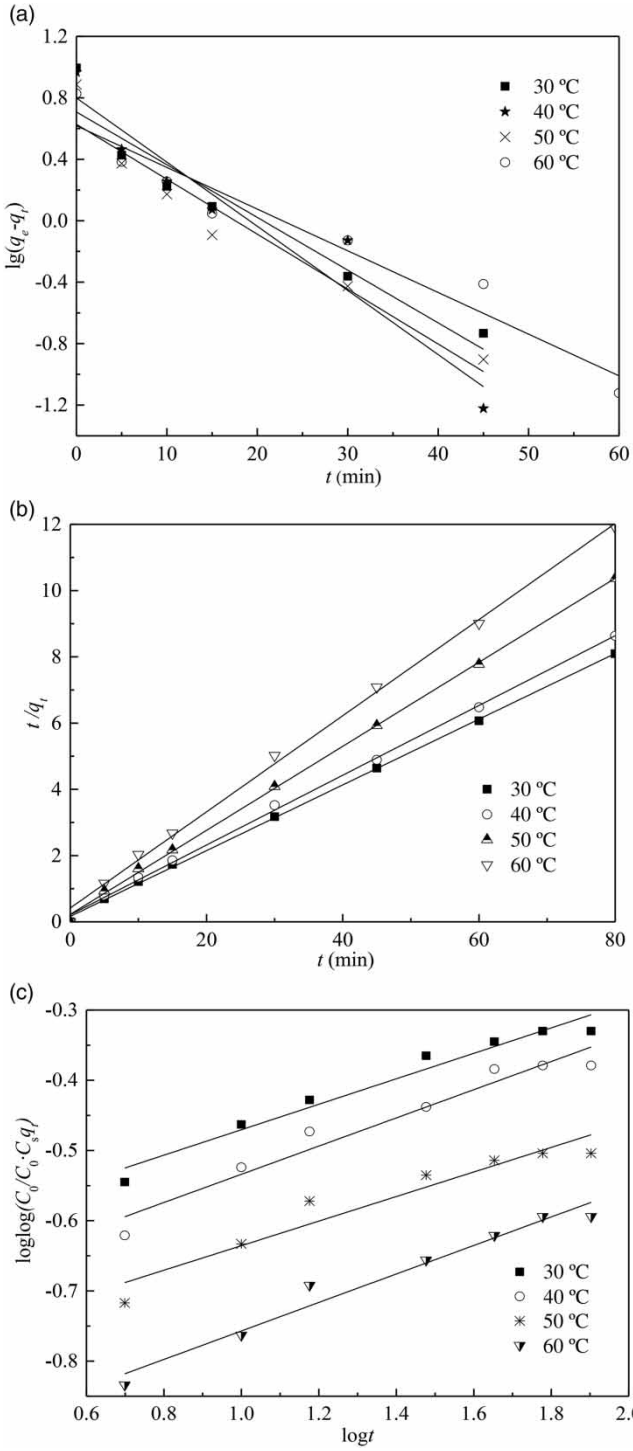


**Figure 2** | Plots of (a) pseudo-first-order, (b) pseudo-second-order, and (c) Bangham kinetic models under different temperatures.

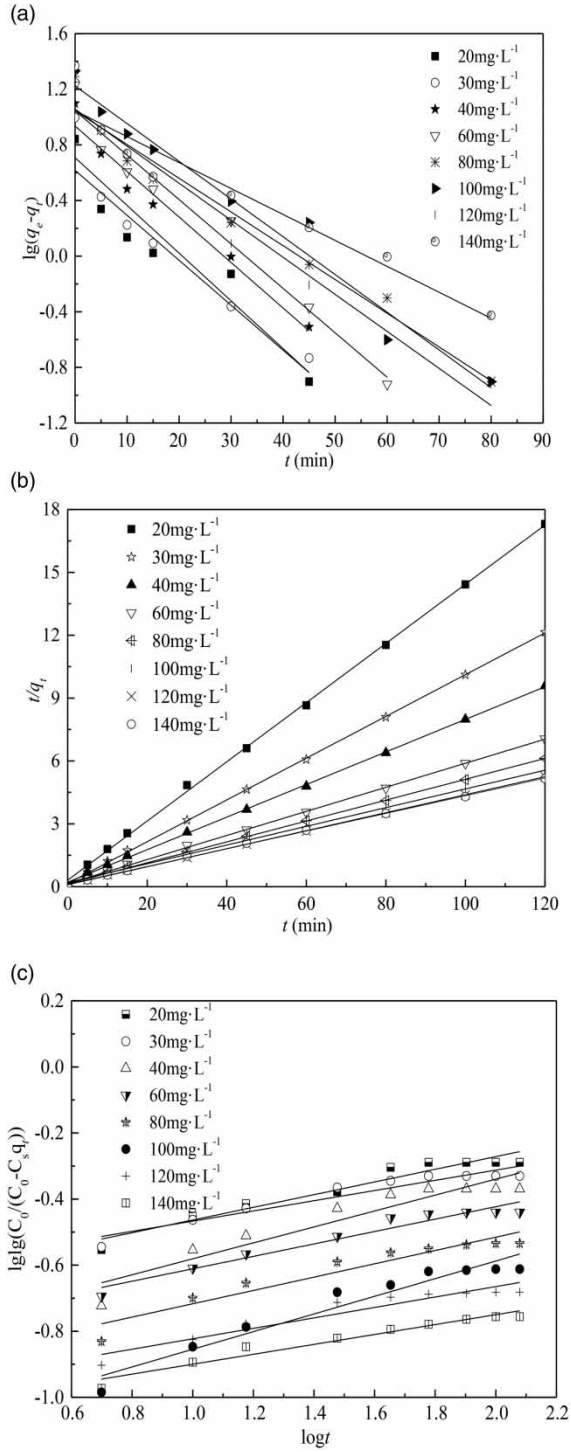


**Figure 3** | Plots of (a) pseudo-first-order, (b) pseudo-second-order, and (c) Bangham kinetic models under different concentrations.

**Table 1** | Adsorption kinetic constants under different temperatures

| | Pseudo-first-order | | | Pseudo-second-order | | | Bangham | | | |
|---|---|---|---|---|---|---|---|---|---|---|
| T (°C) | $q_e$ (mg·g$^{-1}$) | $k_1$ (min$^{-1}$) | $R^2$ | $q_e$ (mg·g$^{-1}$) | $k_2$ (g·mg$^{-1}$·min$^{-1}$) | $R^2$ | $k_0$ | $\alpha$ | $R^2$ | $q_{e,exp}$ (mg·g$^{-1}$) |
| 30 | 5.11 | 0.079 | 0.9068 | 10.08 | 0.0598 | 0.9991 | 0.0257 | 0.1813 | 0.9541 | 9.89 |
| 40 | 6.30 | 0.096 | 0.9093 | 9.50 | 0.0521 | 0.9984 | 0.0212 | 0.2008 | 0.9390 | 9.27 |
| 50 | 4.25 | 0.082 | 0.9219 | 7.88 | 0.0716 | 0.9990 | 0.0178 | 0.1749 | 0.9077 | 7.72 |
| 60 | 4.15 | 0.062 | 0.9270 | 6.89 | 0.0505 | 0.9970 | 0.0126 | 0.2029 | 0.9610 | 6.72 |

**Table 2** | Adsorption kinetic constants under different concentrations

| | Pseudo-first-order | | | Pseudo-second-order | | | Bangham | | | |
|---|---|---|---|---|---|---|---|---|---|---|
| Concentration (mg·L$^{-1}$) | $q_e$ (mg·g$^{-1}$) | $k_1$ (min$^{-1}$) | $R^2$ | $q_e$ (mg·g$^{-1}$) | $k_2$ (g·mg$^{-1}$·min$^{-1}$) | $R^2$ | $k_0$ | $\alpha$ | $R^2$ | $q_{e,exp}$ (mg·g$^{-1}$) |
| 20 | 4.14 | 0.0744 | 0.8826 | 7.08 | 0.0645 | 0.9992 | 0.0255 | 0.1918 | 0.9273 | 6.94 |
| 30 | 5.11 | 0.0791 | 0.9068 | 10.04 | 0.0640 | 0.9996 | 0.0276 | 0.1543 | 0.9071 | 9.89 |
| 40 | 8.62 | 0.0753 | 0.9598 | 12.87 | 0.0283 | 0.9990 | 0.0174 | 0.2411 | 0.8770 | 12.53 |
| 60 | 11.11 | 0.0736 | 0.9615 | 17.42 | 0.0223 | 0.9991 | 0.0183 | 0.1880 | 0.9402 | 17.00 |
| 80 | 11.10 | 0.0559 | 0.9638 | 20.08 | 0.0171 | 0.9992 | 0.0139 | 0.2016 | 0.9011 | 19.60 |
| 100 | 16.75 | 0.0625 | 0.9678 | 22.42 | 0.0098 | 0.9977 | 0.0087 | 0.2671 | 0.9275 | 21.53 |
| 120 | 11.40 | 0.0614 | 0.9540 | 23.31 | 0.0192 | 0.9995 | 0.0120 | 0.1580 | 0.9000 | 22.84 |
| 140 | 11.11 | 0.0430 | 0.9110 | 23.75 | 0.0144 | 0.9989 | 0.0103 | 0.1499 | 0.9469 | 23.28 |

## Adsorption mechanism

The pseudo-second-order model, containing all the rate controlling processes of adsorption, such as surface adsorption, intra-particle diffusion, and so on, could not truly reflect the mechanism of this adsorption process (Zhang *et al.* 2019). In order to further explain the adsorption mechanism, the adsorption behavior of Ni(II) by CAMCBs at different temperatures was subjected to the intra-particle diffusion equation (Moussavi & Khosravi 2011).

$$q_t = k_{id} t^{1/2} + C \tag{8}$$

where $k_{id}$ (mg·g$^{-1}$·min$^{1/2}$) is the internal diffusion coefficient.

Plots and calculated parameters of the intra-particle diffusion model under different temperatures are shown in Figure 4 and Table 3, respectively. According to Figure 4, the plots were straight lines that didn't intersect the origin. This finding demonstrated that the adsorption of Ni(II) onto CAMCBs was not solely controlled by the intra-particle diffusion and that membrane diffusion processes might be involved (Vimonses *et al.* 2009), which was consistent with the conclusion obtained by the Bangham model. The

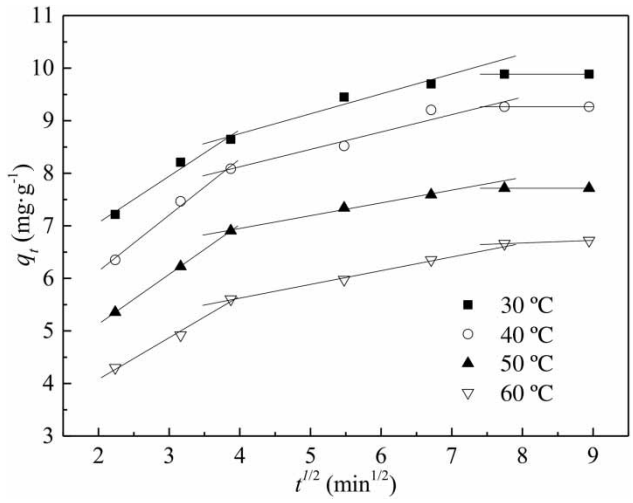


**Figure 4** | Intra-particle diffusion model plot at various temperatures.

**Table 3** | Intra-particle diffusion model kinetic constants for the adsorption at various temperatures

| T (°C) | $k_1$ (mg·g$^{-1}$·min$^{1/2}$) | $k_2$ (mg·g$^{-1}$·min$^{1/2}$) | $k_3$ (mg·g$^{-1}$·min$^{1/2}$) | $C_1$ | $C_2$ | $C_3$ | $R_1^2$ | $R_2^2$ | $R_3^2$ |
|---|---|---|---|---|---|---|---|---|---|
| 30 | 0.88 | 0.32 | 0 | 5.29 | 7.53 | 9.89 | 0.957 | 0.902 | 1.000 |
| 40 | 1.07 | 0.33 | 0 | 4.00 | 6.80 | 9.27 | 0.985 | 0.919 | 1.000 |
| 50 | 0.95 | 0.21 | 0 | 3.24 | 6.13 | 7.72 | 0.999 | 0.964 | 1.000 |
| 60 | 0.79 | 0.27 | 0.05 | 2.50 | 4.52 | 6.27 | 0.978 | 0.993 | 1.000 |

entire adsorption process was divided into three phases. The first phase was the surface diffusion process (membrane diffusion), that is, the adsorbate diffused to the surface of the adsorbent. The second phase was the intragranular diffusion process, namely the diffusion of the adsorbate in the pores of the adsorbent. The last phase was the adsorption equilibrium stage. In addition, the diffusion rate constants $k_2$ and $k_3$ are much smaller than $k_1$, demonstrating that the surface diffusion proceeded much faster. When the surface of the CAMCBs reached adsorption saturation, Ni(II) entered the internal pores of the adsorbent particles. And then the diffusion resistance gradually increased, resulting in a decrease in diffusion rate and finally reaching adsorption equilibrium (Zhang *et al.* 2019).

## Adsorption isotherms

Equilibrium data, commonly known as adsorption isotherms, describe the relationship between the amount adsorbed by a unit weight of adsorbent and the amount of adsorbate remaining in a test medium at equilibrium. Two kinds of adsorption isotherms, namely Langmuir and Freundlich models, were used to analyze the adsorption data of Ni(II) adsorbed by CAMCBs. The parameters obtained from the different models provide important information on the surface properties of the adsorbent and the affinity of adsorbent to the adsorbate.

Langmuir isotherm assumes that the adsorption process takes place at a surface with homogeneous binding sites, and one site only can be occupied by one molecule of adsorbate, which demonstrated that the adsorption process is monolayer in nature (Chen *et al.* 2010). The essential features of the Langmuir isotherm may be expressed in terms of equilibrium parameter $R_L$, which is a dimensionless constant referred to as a separation factor or equilibrium parameter (Dada *et al.* 2012). The equations of the Langmuir isotherm are represented as follows:

$$\frac{C_e}{q_e} = \frac{1}{q_m K_L} + \frac{C_e}{q_m} \tag{9}$$

$$R_L = \frac{1}{1 + K_L C_0} \tag{10}$$

where $K_L$ (L·mg$^{-1}$) is the Langmuir constant related to the energy of adsorption. If a value for $R_L$ is greater than 1, the adsorption is linear. If the $R_L$ value lies between 0 and 1, the adsorption process is favorable. If a value for $R_L$ is equal to 0, the adsorption process is irreversible (Dada *et al.* 2012).

The Freundlich isotherm is an empirical equation, which is based on the assumption that the adsorption process takes place on a heterogeneous surface through a multilayer adsorption mechanism, and adsorption capacity is relevant to the concentration of Ni(II) at equilibrium (Jalil *et al.* 2010). The equation of the Freundlich isotherm is expressed as follows:

$$\log q_e = \frac{1}{n} \log C_e + \log K_f \tag{11}$$

where $n$ and $K_f$ (mg·g$^{-1}$) are Freundlich constants, which represent adsorption strength and adsorption capacity, respectively. The favorability and the nature of the adsorption process can be identified from the value of $n$. If $n$ lies between 1 and 10, this indicates a favorable sorption process (Toor & Jin 2012).

The experiment data of Ni(II) adsorbed by CAMCBs under a temperature of 30 °C are presented in Figure 5(a). The experiment data were fitted by linear plots of Langmuir and Freundlich adsorption isotherm models as $C_e/q_e$ versus $C_e$ and log $q_e$ versus log $C_e$, respectively (Figure 5(b)

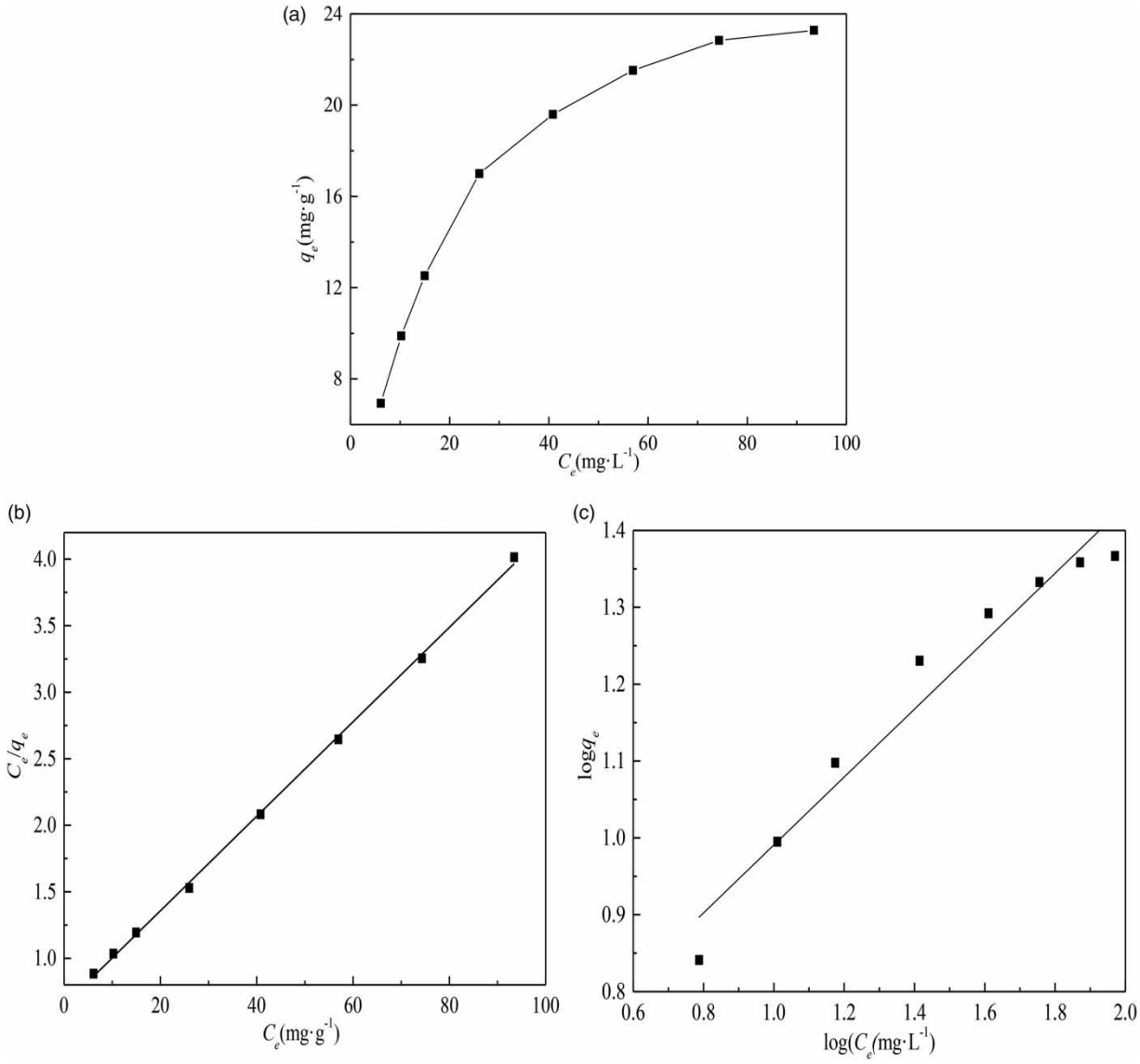


**Figure 5** | (a) Adsorption isotherms, and fitting lines of (b) Langmuir and (c) Freundlich isotherm models.

and 5(c)). Table 3 reports the various parameters obtained from the four isotherm plots mentioned above. As shown in Table 3, the $R^2$ values of Langmuir and Freundlich isotherm models are greater than 0.9, which manifested that both isotherm models fitted very well (Dada *et al.* 2012). The Langmuir isotherm model gave a higher $R^2$ value (0.9991) than the Freundlich isotherm model, which was evidence that the adsorption of Ni(II) on CAMCBs was better fitted by the isotherm model of Langmuir (see Table 4). The applicability of the Langmuir isotherm model demonstrated that the adsorption of Ni(II) on CAMCBs was monolayer adsorption and adsorption occurred at specific homogeneous sites on the adsorbent (Chen *et al.* 2010). In addition, the $R_L$ value (0.3782) of the Langmuir isotherm model was between 0 and 1, and the $n$ value (2.2634) of the Freundlich isotherm model was greater than 1, both indicating that the adsorption process of Ni(II) by CAMCBs was favorable (Dada *et al.* 2012; Toor & Jin 2012).

Furthermore, comparisons of Ni(II) adsorption by different absorbents are given in Table 5. It can be seen that the optimum adsorption temperatures of these adsorbents for adsorbing Ni(II) are between 20 and 30 °C, which are

**Table 4** | Parameters of isotherm models

| Isotherm model | Parameter | Value |
|---|---|---|
| Langmuir | $q_m$ (mg·g$^{-1}$) | 28.17 |
| | $K_L$ (L·mg$^{-1}$) | 0.0548 |
| | $R_L$ | 0.3782 |
| | $R^2$ | 0.9991 |
| Freundlich | $K_f$ (mg·g$^{-1}$) | 3.5408 |
| | $n$ | 2.2634 |
| | $R^2$ | 0.9497 |

**Table 5** | Comparison of our result with other adsorbents

| Adsorbent | Adsorbate | $q_m$ (mg·g$^{-1}$) | Temperature (°C) | Reference |
|---|---|---|---|---|
| Peat | Ni(II) | 6.45 | 25 | Liu *et al.* (2008) |
| Calcareous soils | Ni(II) | 8.57 | 25 ± 2 | Adhami *et al.* (2008) |
| Miscanthus straw biochars | Ni(II) | 11.50 | 20 ± 1 | Shen *et al.* (2018) |
| Rice husk carbon | Ni(II) | 14.45 | 22 | Khan *et al.* (2014) |
| CAMCBs | Ni(II) | 28.17 | 30 | This study |

relatively close to room temperature. All the adsorption behaviors of these adsorbents are consistent with Langmuir. Therefore, the $q_m$ values obtained by linear fitting of Langmuir are compared, and the result reveals that the adsorption capacity of CAMCBs has the best performance.

## Adsorption thermodynamics

Thermodynamic parameters, namely free energy change ($\Delta G$), enthalpy change ($\Delta H$) and entropy change ($\Delta S$), which explain feasibility, spontaneity and nature of adsorbate-adsorbent interactions were calculated using the following equations (Safa Özcan *et al.* 2005):

$$K = \frac{C_0 - C_e}{C_e} \tag{12}$$

$$\Delta G = -RT \ln K \tag{13}$$

$$\ln K = \frac{\Delta S}{R} - \frac{\Delta H}{RT} \tag{14}$$

where $K$ (L·g$^{-1}$) is the distribution coefficient of adsorption equilibrium, and $R$ (8.314 J·mol$^{-1}$·K$^{-1}$) is the universal gas constant.

As shown in Figure 6, the plot of ln$K$ as a function of 1/T yields a straight line. $\Delta H$ and $\Delta S$ were calculated from the slope and the intercept of the plot, respectively. The thermodynamic parameters at various temperatures are presented in Table 6. The $\Delta G$ values were negative over the temperature range 303.15–323.15 K, confirming the feasibility of the process and the spontaneous nature of Ni(II) adsorption on CAMCBs. When the temperature decreased from 323.15 to 303.15 K, the magnitude of $\Delta G$ shifted to a high negative value (from −0.154 to −1.663 kJ·mol$^{-1}$), suggesting that the adsorption of Ni(II) on CAMCBs was rapid and more spontaneous at low temperature (Kara *et al.* 2003). However, at 333.15 K, the value of $\Delta G$ was positive, which showed that the adsorption was no longer a spontaneous one and that the adsorption system gained energy from an external source (Jalil *et al.* 2010). The negative value of $\Delta H$ manifested that the adsorption of Ni(II) on CAMCBs was exothermic (Safa Özcan *et al.* 2005). This was in agreement with the conclusion that the adsorption capacity increased with the decrease of temperature, which was observed in the section above, titled 'Effects of adsorption temperature and adsorption time on adsorption of Ni(II)'. Furthermore, the heat of adsorption was lower than 40 kJ·mol$^{-1}$, indicating that the adsorption of Ni(II) on CAMCBs was physical in origin (Kara *et al.* 2003). In addition, the $\Delta S$ value was negative,

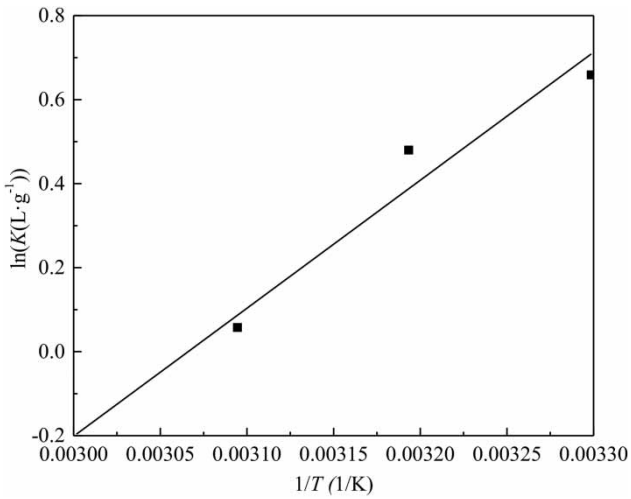


**Figure 6** | Thermodynamic fitting line of Ni(II) adsorption on CAMCBs.

**Table 6** | Thermodynamic parameters for Ni(II) adsorption on CAMCBs

| T(K) | $\Delta G$ (kJ·mol$^{-1}$) | $\Delta H$ (kJ·mol$^{-1}$) | $\Delta S$ (J·mol$^{-1}$·K$^{-1}$) |
|---|---|---|---|
| 303.15 | −1.661 | − 25.338 | − 77.688 |
| 313.15 | −1.249 | | |
| 323.15 | −0.154 | | |
| 333.15 | 0.578 | | |

which demonstrated the decreased randomness at the solid–solution interface during the adsorption of Ni(II) (Kong *et al.* 2017), and the adsorption was a process of entropy reduction.

## Regeneration of used CAMCBs

From the results of Ni(II) adsorption on CAMCBs, it could be concluded that high temperature was favorable for the desorption of Ni(II) in the experimental temperature range from 30 to 60 °C. Besides, CAMCBs was thermo-sensitive, which means it had better desorption at high temperatures than at low temperatures. Therefore, the regeneration of CAMCBs, via the desorption of Ni(II) by using $CaCl_2$ as desorption agent, was investigated at the temperature of 60 °C. In order to explore the effect of $CaCl_2$ concentration on the desorption of Ni(II) on CAMCBs, the CAMCBs after reaching adsorption equilibrium were placed into 20 ml of $CaCl_2$ solution. As shown in Figure 7, the desorption ratio of Ni(II) increased by 21.2% when the $CaCl_2$ concentration increased from 1 to 3 g·L$^{-1}$; however, it only increased by 3.8% when the concentration of $CaCl_2$ increased from 3 to 6 g·L$^{-1}$. Hence, 3 g·L$^{-1}$ was chosen as the concentration of $CaCl_2$ to be used in the subsequent experiments of regeneration. Besides, as shown in Figure 8(a), compared with the

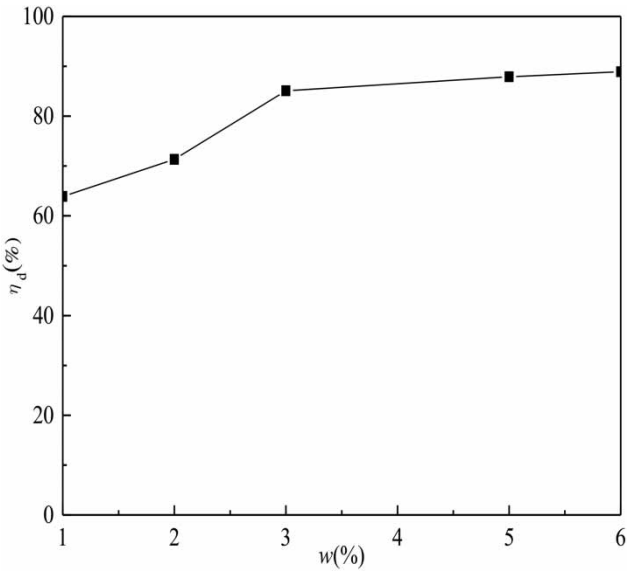


**Figure 7** | Effect of $CaCl_2$ concentration on desorption of Ni(II) on CAMCBs (T = 60 °C, t = 30 min).

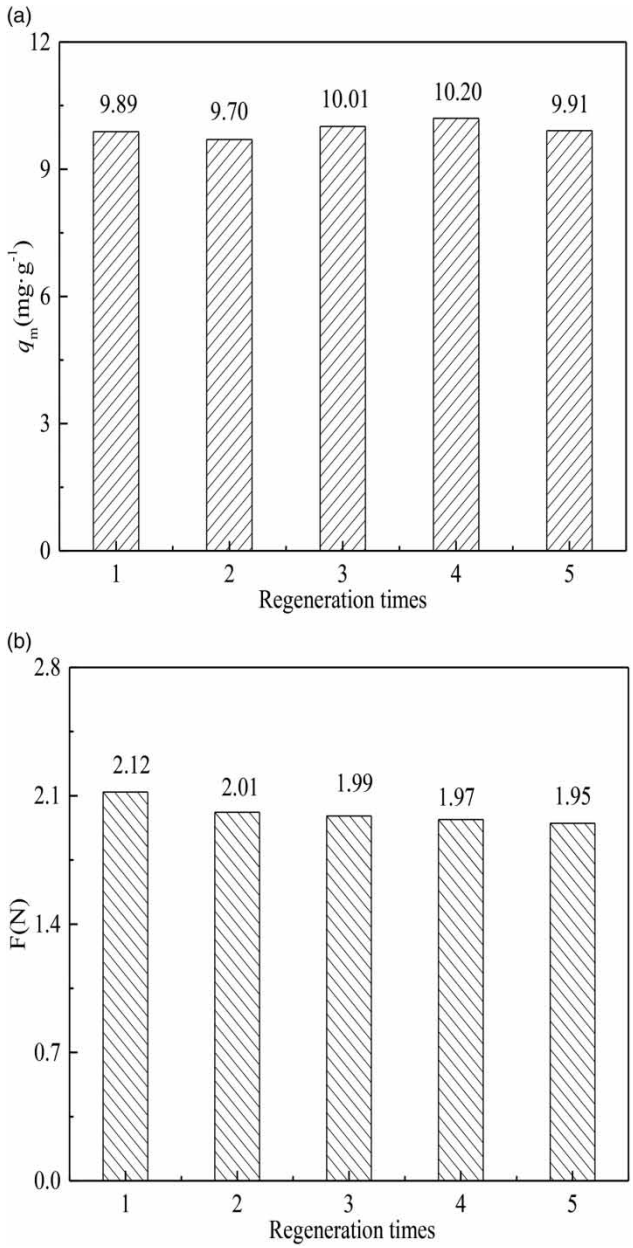


**Figure 8** | Effect of regeneration times on (a) adsorption capacity and (b) mechanical strength of CAMCBs (dosage = 2 g·L$^{-1}$, T = 30 °C, t = 60 min, $C_0$ = 30 mg·L$^{-1}$, and initial pH = 6.9).

adsorption of initial CAMCBs, the adsorption capacity of regenerated CAMCBs in the subsequent four phases showed no obvious change, demonstrating that the CAMCBs had a good regeneration performance. In addition, as shown in Figure 8(b), the mechanical strength of CAMCBs decreased slightly after experiencing five regeneration cycles, indicating that $CaCl_2$ as a desorption agent showed no significant effect on the strength of the CAMCBs structure.

## Characterization of CAMCBs

### SEM analysis

SEM images of CAMCBs before adsorption and after adsorption of Ni(II) are shown in Figure 9. As seen from Figure 9(a), CAMCBs before adsorption had a smooth surface, with obvious fissures and pores. However, after adsorption, the SEM image of CAMCBs exhibited a rough surface, with almost no fissures and pores. The differences of surface morphology between CAMCBs before and after adsorption were mainly due to the covering and filling by the adsorbed Ni(II) on the surface of CAMCBs. In addition, as shown in Figure 9(b), the SEM of CAMCBs after adsorption showed some white particles on the surface, which were likely to be nickel (Jiang *et al.* 2010).

### FT-IR analysis

The FT-IR spectra of CAMCBs before adsorption and after adsorption of Ni(II) are shown in Figure 10. The FT-IR spectra of CAMCBs before and after adsorption showed absorption bands at around 3,448 $cm^{-1}$ (-OH stretching vibration), around 1,636 $cm^{-1}$ (asymmetric -$COO^-$ stretching vibration), and around 1,096 $cm^{-1}$ (C-OH stretching vibration). However, comparing the FT-IR spectra of CAMCBs before and after adsorption, one interesting thing observed was that the peaks of CAMCBs after adsorption shifted slightly to the right, and the intensity of the peaks also increased significantly. The differences of FT-IR spectra between CAMCBs before and after adsorption indicated that -OH, -$COO^-$ and C-OH acted as adsorption sites for Ni(II) on the adsorbent, and Ni(II) was successfully adsorbed on the CAMCBs (Vijaya *et al.* 2008).

## CONCLUSIONS

CAMCBs was found to be an effective adsorbent in the adsorption of Ni(II) from aqueous solution, and the maximum adsorption capacity occurred at the following operation conditions: 2 $g{\cdot}L^{-1}$ adsorbent, 140 $mg{\cdot}L^{-1}$ initial Ni(II) solution, temperature 30 °C, and adsorption time

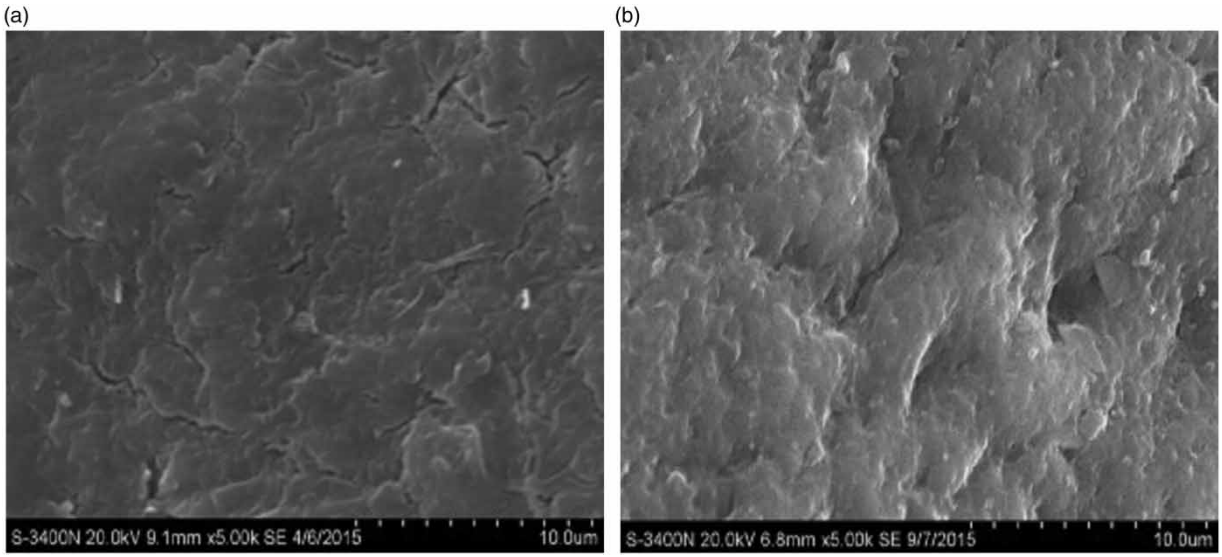


**Figure 9** | SEM images of CAMCBs (a) before adsorption and (b) after adsorption.

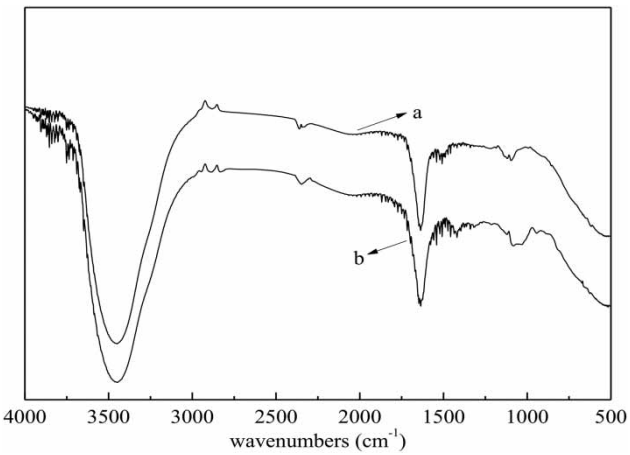


**Figure 10** | FT-IR spectra of CAMCBs (a) before adsorption and (b) after adsorption.

2 h. It was observed that the pseudo-second-order kinetic model was a better fit for the experiment data than the pseudo-first-order kinetic model. The intra-particle diffusion equation was analyzed, indicating that the adsorption process might be controlled by both membrane diffusion and intra-particle diffusion. The best-fit adsorption isotherm was achieved with the Langmuir model, indicating that the behavior of the Ni(II) adsorption process on CAMCBs was monolayer adsorption and that adsorption occurred at specific homogeneous sites on the adsorbent. Furthermore, according to the Langmuir model, the adsorbent's greatest adsorption capacity was predicted to be 28.17 mg·g$^{-1}$ for Ni(II). The negative $\Delta H$ for the adsorption process confirmed the exothermic nature of the adsorption, and the negative value of $\Delta G$ showed the feasibility and spontaneity of Ni(II) adsorption on CAMCBs at 30 to 50 °C. The regeneration results demonstrated the excellent regeneration performance of CAMCBs. Hence, from the foregoing results, it can be safely concluded that CAMCBs is an effective potential adsorbent for removing Ni(II) from wastewater.

## ACKNOWLEDGEMENTS

Financial support from National Natural Science Foundation of China (21667004) and Guangxi Science Foundation Funded Project (2018GXNSFAA281343, 2018GXNSFAA138039), and Ministry-province Jointly-constructed Cultivation Base for State Key Laboratory of Processing for Non-ferrous Metal and Featured Materials in Guangxi Zhuang Autonomous Region (GXKFJ16-06, GXKFJ16-04) is gratefully acknowledged.

## REFERENCES

Adhami, E., Salmanpour, A., Omidi, A., Khosravi, N., Ghasemi-Fasaei, A. & Maftoun, M. 2008 Nickel adsorption characteristics of selected soils as related to some soil properties. *J. Soil. Contam.* **17** (6), 11.

Chen, S., Zhang, J., Zhang, C., Yue, Q., Li, Y. & Li, C. 2010 Equilibrium and kinetic studies of methyl orange and methyl violet adsorption on activated carbon derived from *Phragmites australis*. *Desalination* **252**, 149–156.

Dada, A. O., Olalekan, A. P., Olatunya, A. M. & Dada, O. 2012 Langmuir, Freundlich, Temkin and Dubinin–Radushkevich isotherms studies of equilibrium sorption of $Zn^{2+}$ onto phosphoric acid modified rice husk. *J. Appl. Chem.* **3**, 38–45.

Depci, T., Kul, A. R. & Önal, Y. 2012 Competitive adsorption of lead and zinc from aqueous solution on activated carbon prepared from Van apple pulp: study in single and multi-solute systems. *Chem. Eng. J.* **200–202**, 224–236.

Hong, H. J., Ryu, J., Park, I. S., Ryu, T., Chung, K.-S. & Kim, B.-G. 2016 Investigation of the strontium (Sr(II)) adsorption of an alginate microsphere as a low-cost adsorbent for removal and recovery from seawater. *J. Environ. Manage.* **165**, 263–270.

Jalil, A. A., Triwahyono, S., Adam, S. H., Rahim, N. D., Aziz, M. A. A., Hairom, N. H. H., Razali, N. A. M., Abidin, M. A. Z. & Mohamadiah, M. K. A. 2010 Adsorption of methyl orange from aqueous solution onto calcined Lapindo volcanic mud. *J. Hazard. Mater.* **181**, 755–762.

Jiang, M. Q., Jin, X. Y., Lu, X. Q. & Chen, Z.-L. 2010 Adsorption of Pb(II), Cd(II), Ni(II) and Cu(II) onto natural kaolinite clay. *Desalination* **252**, 33–39.

Kara, M., Yuzer, H., Sabah, E. & Celik, M. S. 2003 Adsorption of cobalt from aqueous solutions onto sepiolite. *Water Res.* **37**, 224–232.

Kara, I., Yilmazer, D. & Akar, S. T. 2017 Metakaolin based geopolymer as an effective adsorbent for adsorption of zinc(II) and nickel(II) ions from aqueous solutions. *Appl. Clay Sci.* **139**, 54–63.

Khan, T., Isa, M. H., Chaudhuri, M., Muhammad, R. U. M. & Saeed, M. O. 2014 Determination of adsorption capacity of agricultural-based carbon for Ni (II) adsorption from aqueous solution. *Appl. Mech. Mater.* **567**, 20–25.

Kong, Q., He, X., Shu, L. & Miao, M.-S. 2017 Ofloxacin adsorption by activated carbon derived from luffa sponge: kinetic, isotherm, and thermodynamic analyses. *Process Saf. Environ.* **112**, 254–264.

Li, Z., Yao, Y., Wei, G., Jiang, W., Wang, Y. & Zhang, L. 2016 Adsorption and heat-energy-aid desorption of cationic dye on a new thermo-sensitive adsorbent: methyl cellulose/calcium alginate beads. *Polym. Eng. Sci.* **56**, 1382–1389.

Li, Z. M., Wu, W. W., Jiang, W. Y., Zhang, L. Y., Li, Y. S., Tan, Y. Y., Chen, S. H., Lv, M. G., Luo, F. H., Luo, T. W. & Wei, G. T. 2019 Preparation and regeneration of a thermo-sensitive adsorbent material: methyl cellulose/calcium alginate beads (MC/CABs). *Polym. Bull.* **76**, 1–22.

Liao, B., Sun, W. Y., Guo, N., Ding, S.-I. & Su, S.-J. 2016 Equilibriums and kinetics studies for adsorption of Ni(II) ion on chitosan and its triethylenetetramine derivative. *Colloid Surface A* **501**, 32–41.

Liu, Z., Zhou, L., Wei, P., Zeng, K., Wen, C.-X. & Lan, H.-H. 2008 Competitive adsorption of heavy metal ions on peat. *J. China Univ. Mining Technol.* **18** (2), 255–260.

Moino, B. P., Costa, C. S. D., Silva, M. G. C. D. & Vieira, M. G. A. 2017 Removal of Ni(II) on residue of alginate extraction from *Sargassum filipendula* seaweed in packed bed. *Can. J. Chem. Eng.* **95**, 2120–2128.

Moussavi, G. & Khosravi, R. 2011 The removal of cationic dyes from aqueous solutions by adsorption onto pistachio hull waste. *Chem. Eng. Res. Des.* **89** (10), 2182–2189.

Namasivayam, C. & Sangeetha, D. 2006 Removal and recovery of vanadium(V) by adsorption onto zncl$_2$ activated carbon: kinetics and isotherms. *Adsorption* **12** (2), 103–117.

Ren, H., Gao, Z., Wu, D., Jiang, J., Sun, Y. & Luo, C. 2016 Efficient Pb(II) removal using sodium alginate–carboxymethyl cellulose gel beads: preparation, characterization, and adsorption mechanism. *Carbohyd. Polym.* **137**, 402–409.

Romera, E., González, F., Ballester, A., Blázquez, M. L. & Muñoz, J. A. 2007 Comparative study of biosorption of heavy metals using different types of algae. *Bioresource Technol.* **98**, 3344.

Safa Özcan, A., Erdem, B. & Özcan, A. 2005 Adsorption of Acid Blue 193 from aqueous solutions onto BTMA-bentonite. *Colloid Surface A* **266**, 73–81.

Shen, Z., Zhang, Y., Jin, F., Alessi, D. S., Zhang, Y., Wang, F., McMillan, O. & Al-Tabbaa, A. 2018 Comparison of nickel adsorption on biochars produced from mixed softwood and Miscanthus straw. *Environ. Sci. Pollut. Res. Int.* **25** (15), 1–10.

Stender, E. G. P., Khan, S., Ipsen, R., Madsen, F., Hägglund, P., Hachem, M. A., Almdal, K., Westh, P. & Svensson, B. 2018 Effect of alginate size, mannuronic/guluronic acid content and pH on particle size, thermodynamics and composition of complexes with $\beta$-lactoglobulin. *Food Hydrocolloid.* **75**, 157–163.

Toor, M. & Jin, B. 2012 Adsorption characteristics, isotherm, kinetics, and diffusion of modified natural bentonite for removing diazo dye. *Chem. Eng. J.* **187**, 79–88.

Vijaya, Y., Popuri, S. R., Boddu, V. M. & Krishnaiah, A. 2008 Modified chitosan and calcium alginate biopolymer sorbents for removal of nickel(II) through adsorption. *Carbohyd. Polym.* **72**, 261–271.

Vimonses, V., Lei, S., Jin, B., Chow, C. W. K. & Saint, C. 2009 Kinetic study and equilibrium isotherm analysis of Congo Red adsorption by clay materials. *Chem. Eng. J.* **148** (2–3), 354–364.

Volesky, B. 1987 Biosorbents for metal recovery. *Trends Biotechnol.* **5**, 96–101.

Xu, M., Liu, J., Hu, K., Xu, C. & Fang, Y. 2016 Nickel(II) removal from water using silica-based hybrid adsorbents: fabrication and adsorption kinetics. *Chinese J. Chem. Eng.* **24** (10), 1353–1359.

Xu, J., Zhang, C., Ge, T., Dai, Y. & Weng, R. 2018 Performance study of sodium alginate-nonwoven fabric composite membranes for dehumidification. *Appl. Therm. Eng.* **128**, 214–224.

Zhang, L. Y., Xin, Z. W., Fei, X. Y., Luo, H. Y., Li, H. Y., Lu, B. X., Li, Z. M. & Wei, G. T. 2019 Study on adsorption of tetracycline by red mud-based ceramsite. *J. Water Supply Res. T.* **68**, 39–50.

Zhao, Y., Xu, L., Liu, M., Duan, Z. & Wang, H. 2018 Magnetic mesoporous thiourea-formaldehyde resin as selective adsorbent: a simple and highly-sensitive electroanalysis strategy for lead ions in drinking water and milk by solid state-based anodic stripping. *Food Chem.* **239**, 40.

Zhou, Z., Kong, D., Zhu, H., Wang, N., Wang, Z., Wang, Q., Liu, W., Li, Q., Zhang, W. & Ren, Z. 2017 Preparation and adsorption characteristics of an ion-imprinted polymer for fast removal of Ni(II) ions from aqueous solution. *J. Hazardous Mater.* **341**, 355.

First received 24 October 2018; accepted in revised form 1 July 2019. Available online 16 August 2019